

Cortical energy demands of signaling and nonsignaling components in brain are conserved across mammalian species and activity levels

Fahmeed Hyder^{a,b,c,1}, Douglas L. Rothman^{a,b,c}, and Maxwell R. Bennett^d

^aMagnetic Resonance Research Center (MRRC) and Departments of ^bDiagnostic Radiology and ^cBiomedical Engineering, Yale University, New Haven, CT 06520; and ^dBrain and Mind Research Institute, University of Sydney, Sydney, NSW 2050, Australia

Edited* by Robert G. Shulman, Yale University School of Medicine, New Haven, CT, and approved November 29, 2012 (received for review August 28, 2012)

The continuous need for ion gradient restoration across the cell membrane, a prerequisite for synaptic transmission and conduction, is believed to be a major factor for brain's high oxidative demand. However, do energy requirements of signaling and non-signaling components of cortical neurons and astrocytes vary with activity levels and across species? We derived oxidative ATP demand associated with signaling (P_s) and nonsignaling (P_{ns}) components in the cerebral cortex using species-specific physiologic and anatomic data. In rat, we calculated glucose oxidation rates from layer-specific neuronal activity measured across different states, spanning from isoelectricity to awake and sensory stimulation. We then compared these calculated glucose oxidation rates with measured glucose metabolic data for the same states as reported by 2-deoxy-glucose autoradiography. Fixed values for P_s and P_{ns} were able to predict the entire range of states in the rat. We then calculated glucose oxidation rates from human EEG data acquired under various conditions using fixed P_s and P_{ns} values derived for the rat. These calculated metabolic data in human cerebral cortex compared well with glucose metabolism measured by PET. Independent of species, linear relationship was established between neuronal activity and neuronal oxidative demand beyond isoelectricity. Cortical signaling requirements dominated energy demand in the awake state, whereas nonsignaling requirements were ~20% of awake value. These predictions are supported by ^{13}C magnetic resonance spectroscopy results. We conclude that mitochondrial energy support for signaling and nonsignaling components in cerebral cortex are conserved across activity levels in mammalian species.

spike rate | field potentials | glutamate | functional MRI | bispectral index

The brain is one of the most energy demanding tissues in the body (1). ^{13}C magnetic resonance spectroscopy (MRS) in the rat has shown that, in the resting awake state, ~80% of cortical energy consumption is used to support signaling as reflected by the rate of glutamate neurotransmitter release and astroglial uptake (2, 3). Cerebral energy demand is also positively correlated with the rate of pyramidal neuron firing in rat cortex (4, 5). ^{13}C MRS findings in the human cortex have been generally consistent with the rat results (6). However, there remain questions as to how well the energy costs of specific subcellular processes needed to support synaptic transmission and conduction are conserved over different activity levels and/or across species.

Recent bottom-up energy budgets for gray matter in the mammalian brain have attempted to understand the energetic costs of neuronal and glial electrical and neurotransmission events occurring in the neuropil (7, 8) by calculating the ATP used per neuron for signaling (P_s) and nonsignaling (P_{ns}) events. In the awake cortex, the total ATP used per unit cortical volume per unit time (E_{tot} ; in units of ATP/s per centimeter³) was determined by multiplying the P_s (in units of ATP/neuron per spike) and P_{ns} (in units of ATP/neuron per second) parameters with cellular densities (η) and average cortical firing rates ($\langle f \rangle$) to give signaling (E_s) and nonsignaling (E_{ns}) components,

$$E_{\text{tot}} = E_s + E_{ns} = \sum P_s \langle f \rangle + \sum P_{ns} \eta, \quad [1]$$

where the summation spans for neurons and astrocytes. These studies agreed with *in vivo* measurements in that the majority of brain energy consumption was used to support signaling and also concluded that both signaling and nonsignaling events in human were about two to three times more costly on a per neuron basis than in the rat. However, these budgets have limitations (7, 8); most notably, the histological and biophysical parameters used disagree with recent values, heterogeneity across cortical lamina was disregarded (9–11), and the comparison was made with only one the resting awake state.

Here, we use a top-down as opposed to a bottom-up approach to assess the fundamental links between electrical and chemical events at the neuropil. We tested the hypotheses that the energy requirements per cell for signaling (P_s) and nonsignaling (P_{ns}) are independent of the state of neuronal activity (e.g., sensory activation, awake, asleep, or anesthetized) and are conserved across species (i.e., rat and human). We used layer-specific morphologic, neurophysiologic, and metabolic data in rat brain to calculate P_s and P_{ns} , which were then tested on human data. In contrast to views highlighting differences between rat and human brain neurometabolic couplings (7, 8), our results suggest that, on a per cellular basis, the mitochondrial energy support for mammalian cortical functions during signaling and nonsignaling are conserved.

Calculations

Energetics of Signaling and Nonsignaling Components. We did not sum bottom-up contributions to total oxidative ATP demand as previously done in other budgets (7, 8) but rather, tested whether unchanging values of P_s and P_{ns} can account for measured *in vivo* results over a range of cortical activity levels (*SI Text*, section 1 and Tables S1 and S2). Although the E_s term in Eq. 1 encompasses function of both neurons and astrocytes, we base our budget to neuronal activity data due to limited ability to quantify astrocytic signaling. Given that neuronal firing is statistically representative of neuropil activity (12), we used spike rate as a quantitative measure of cortical function as has been done before (7, 8). In Eq. 1, $\langle f \rangle$ is given in units of spike.neuron/cm³ and η_N and η_A are given in units of cells/cm³. Tables S1 and S2 list values of neuronal activity and glucose consumption in rat and human, respectively (*SI Text*, section 1). Recordings of cortical signaling were reflected by layer-specific microelectrodes in rats and EEG in humans, whereas metabolic

Author contributions: F.H., D.L.R., and M.B. designed research, performed research, analyzed data, and wrote the paper.

The authors declare no conflict of interest.

*This Direct Submission article had a prearranged editor.

See Commentary on page 3216.

¹To whom correspondence should be addressed. E-mail: fahmeed.hyder@yale.edu.

This article contains supporting information online at www.pnas.org/lookup/suppl/doi:10.1073/pnas.1214912110/-DCSupplemental.

measurements were made by 2-deoxyglucose (2DG) autoradiography in rats and fluoro-deoxyglucose PET in humans.

Energetics of Signaling from Layer-Specific Neuronal Recordings in the Rat Somatosensory Cortex. Cortical signaling involves events like dendritic depolarization, axonal propagation, vesicular endocytosis and exocytosis, neurotransmitter cycling, ionotropic and metabotropic receptor activity, etc. To determine E_s in Eq. 1, we first multiplied the spike rate of the i th cortical layer (f_i in units of spike/s) by the cortical density in the same layer ($\eta_{N,i}$ in units of neurons/cm³) to obtain the number of firing events per unit volume ($f_i \eta_{N,i}$ in units of spike.neuron/s per centimeter³). Next, we estimated the fraction of the i th cortical layer in relation to the entire cortical thickness ($\delta_i/\Sigma\delta_j$). On multiplying, these two terms and summing across all layers gives $\langle f \rangle$ in Eq. 1 (in units of spike.neuron/s per centimeter³):

$$\langle f \rangle = \sum (\delta_i f_i \eta_{N,i}) / \sum \delta_j \quad [2]$$

Using values of δ , η , and f from recent studies, we then determined if Eq. 1 was able to fit results from experimentally measured regional metabolism across different activity levels.

Energetics of Nonsignaling Events from Isoelectric Condition in the Rat Somatosensory Cortex. We assigned the nonsignaling energy primarily to ion movement associated with maintaining neuronal and glial resting potentials described by Eq. 1. To separately calculate $P_{ns,A}$ and $P_{ns,N}$, we needed input resistances of neurons ($R_{in,N}$) and astrocytes ($R_{in,A}$), which describe the energy demand of leaky cell membranes at rest (*SI Text*, section 2, and Fig. S1) and the average neuronal (η_N) and astrocytic (η_A) densities in the cerebral cortex (Table 1). Because recent $R_{in,x}$ and η_x measurements in the rat show that values for neurons and astrocytes are quite similar (13–16), the calculations were slightly simplified by assuming that $R_{in,N} \sim R_{in,A}$ and $\eta_N \sim \eta_A$ (Table 1 and *SI Text*, section 2). To determine P_{ns} , we needed the metabolic demand for nonsignaling, which was possible for the rat, because state of deep pentobarbital anesthesia in Table S1 induces an isoelectric condition and thus, just contains the E_{ns} term. Because neuronal recordings do not show any significant cortical activity in the pentobarbital state, the nonsignaling energy described was uniform across all layers. By multiplying P_{ns} (in units of ATP/cell per second) with η_x (in units of cells/cm³), we get E_{ns} in Eq. 1 (in units of ATP/s per centimeter³). This empirically derived E_{ns} was held constant for all other states.

Table 1. Energy budget parameters in rat and human brains

Source	η_N	η_A	$R_{in,N}$	$R_{in,A}$	$P_{ns,N}$	$P_{ns,A}$	P_s
This study (rat)	4.75*	4.75*	74 [†]	74 [†]	9.20 [‡]	6.85 [‡]	4.81 [§]
This study (human)	1.83*	1.83*	74 [†]	74 [†]	9.20 [‡]	6.85 [‡]	4.81 [§]
Ref. 7 (rat)	9.2	9.2	200	500	3.42	1.02	0.71
Ref. 8 (human)	4.0	3.8	79	163	8.6	3.1	2.4

Average values of cortical density of neurons ($\eta_N \times 10^7$ neuron/cm³) and astrocytes ($\eta_A \times 10^7$ astrocyte/cm³) densities, input resistances of neurons ($R_{in,N}; M\Omega$) and astrocytes ($R_{in,A}; M\Omega$), rate of ATP use for nonsignaling per neuron ($P_{ns,N} \times 10^8$ ATP/neuron per second) and astrocyte ($P_{ns,A} \times 10^8$ ATP/astrocytes per second), and ATP use per signaling event per neuron ($P_s \times 10^9$ ATP/spike per neuron).

*Table 2 in ref. 15 shows average cortical neuronal density in rat brain, figure 2 in ref. 16 shows neuron vs. astrocyte densities are similar, and figure 2a in ref. 17 shows rat and human neuronal densities differ by ~2.6.

[†]Estimated from Fig. S1A.

[‡]Calculated from Eq. S1 and Eq. 5 (details in Fig. S1B).

[§]Calculated from Eqs. 1–6.

Converting Calculated Total ATP Production Rate to Cerebral Glucose Oxidation Rate. We used the following formula to convert E_{tot} in Eq. 1 to rate of glucose oxidation [calcCMR_{glc(ox)}],

$$\text{calcCMR}_{\text{glc(ox)}} = k E_{\text{tot}}, \quad [3]$$

where k depends on the oxygen-to-glucose index (OGI), which is given by the ratio of cerebral metabolic rates of oxygen (CMR_{O₂}) and glucose (CMR_{glc}) consumption, and k itself is given by $10^7 / (A_{vo} \rho \text{ OGI})$, where ρ is the tissue density (1.05 g/mL) and A_{vo} is the Avogadro constant ($6.023 \times 10^{23}/\text{mol}$). Similarly, the measured glucose oxidation [measCMR_{glc(ox)}] was given by

$$\text{measCMR}_{\text{glc(ox)}} = \frac{1}{6} \times \text{OGI} \times \text{measCMR}_{\text{glc}}, \quad [4]$$

where measCMR_{glc} was obtained from 2DG autoradiography in rats and fluoro-deoxyglucose PET in humans (Tables S1 and S2); it is given by sum of oxidative [CMR_{glc(ox)}] and nonoxidative [CMR_{glc(nonoxy)}] terms, whereas CMR_{glc(ox)} itself has neuronal [CMR_{glc(ox),N}] and astrocytic [CMR_{glc(ox),A}] components. Thus, it is possible to obtain calculated forms of CMR_{glc(nonoxy)}, CMR_{glc(ox),N}, and CMR_{glc(ox),A} across all activity states. Finally, we compared calcCMR_{glc(ox)} with measCMR_{glc(ox)} by least-square fitting to determine P_s and P_{ns} :

$$\sigma^2 = \sum [\text{calcCMR}_{\text{glc(ox)},i} - \text{measCMR}_{\text{glc(ox)},i}]^2, \quad [5]$$

where summation was over all states (Tables S1 and S2).

Calculating Signaling and Nonsignaling Energetics in the Human Visual Cortex. To test whether $P_{ns,N}$, $P_{ns,A}$, and P_s derived from the rat (Table 1) were representative of those values in human cerebral cortex, we calculated E_{ns} in the human by simply multiplying the $P_{ns,N}$ and $P_{ns,A}$ terms with η_N and η_A , respectively [i.e., cellular density is about 2.6 times lower in human vs. rat (17)]. Neuronal activity for each state in the human was represented by EEG-measured bispectral index (BIS) values ranging from 0 to 100 (Table S2) as used intraoperatively (18). We calculated the E_s term in the human similarly as in the rat, but because the neuronal activity data in the human originated from EEG recordings (*SI Text*, section 3), additional steps were needed to represent Eq. 2 to convert the BIS into units similar to the rat data (i.e., in units of spike.neuron/s per centimeter³):

$$\langle f \rangle_{\text{human}} = (f_{BIS}/f_{BIS,AR}) (\eta_{N,\text{human}}/\eta_{N,\text{rat}}) \times \left(\sum (\delta_i f_i \eta_{N,i})_{\text{rat},\text{AR}} / \left(\sum \delta_j \right)_{\text{human}} \right). \quad [6]$$

f_{BIS} and $f_{BIS,AR}$ are BIS values for a given state and the awake condition (Table S2), $\eta_{N,\text{human}}$ and $\eta_{N,\text{rat}}$ are the average neuronal densities in the human and rat cortices (Table 1), $\sum (\delta_i f_i \eta_{N,i})_{\text{rat},\text{AR}}$ is the numerator of Eq. 2 for the awake condition in the rat (Table 2), and $(\sum \delta_j)_{\text{human}}$ is the cortical thickness in the human (Table 3). This conversion, from f_{BIS} scale in humans to $\langle f \rangle$ scale in rats, accounts for differences in average neuronal density and cortical thickness between rat somatosensory and human visual cortices (15–17, 19).

Results

P_s in the Rat Somatosensory Cortex. The averaged representation of normalized activity of neurons across all states showed dominant activity in the bottom two-thirds of cortical layers (Fig. S2 and Table S1), which is in good agreement with prior studies that investigated layer-specific representation of neuronal activity, 2DG autoradiography, and functional MRI (fMRI) data (9–11). The laminar activity was then used with Eqs. 1–6 to derive calcCMR_{glc(ox)} and compared with measCMR_{glc(ox)} by least-

Table 2. Calculated CMR_{glc(ox)} derived from neuronal activity in rat somatosensory cortex for OGI of 5.6

Behavioral state*	PR	UR1 [†]	US1 [†]	AR [†]	AS [†]	UR2 [‡]	US2 [‡]	CR [‡]	CS [‡]	HR [‡]	HS [‡]
$\Sigma(\delta_i f_i \eta_{N,i}) (\times 10^3 \text{ spike.neuron.cm}^3 \text{ per centimeter}^3)$	0.00	7,051	9,393	8,858	9,090	6,024	8,629	4,233	6,677	5,213	5,533
$\Sigma(\delta_i f_i \eta_{N,i})/\Sigma\delta_j (\times 10^7 \text{ spike.neuron.s per centimeter}^3)$	0.00	3.71	4.95	4.67	4.79	13.36	19.13	9.39	14.80	11.56	12.27
$E_{ns} = \Sigma P_{ns,x} \times \eta_{N,x} (\times 10^{17} \text{ ATP/s per centimeter}^3)$	0.76	0.76	0.76	0.76	0.76	0.76	0.76	0.76	0.76	0.76	0.76
$E_s = P_s \times \Sigma(\delta_i f_i \eta_{N,i})/\Sigma\delta_j (\times 10^{17} \text{ ATP/s per centimeter}^3)$	0.00	1.79	2.38	2.24	2.30	1.53	2.19	1.07	1.69	1.32	1.40
$E_{tot} = E_{ns} + E_s (\times 10^{17} \text{ ATP/s per centimeter}^3)$	0.76	2.55	3.14	3.01	3.07	2.29	2.95	1.84	2.45	2.08	2.16
calcCMR _{glc(ox)} ($\mu\text{mol/g per minute}$)	0.22	0.72	0.89	0.85	0.87	0.65	0.83	0.52	0.69	0.59	0.61
measCMR _{glc(ox)} ($\mu\text{mol/g per minute}$)	0.20	0.63	0.90	0.82	0.91	0.63	0.90	0.49	0.68	0.61	0.63

Details in *Calculations*. The calculated CMR_{glc(ox)} [calcCMR_{glc(ox)}] was determined from Eq. 3. The measured CMR_{glc(ox)} [measCMR_{glc(ox)}] was determined from Eq. 4 assuming OGI of 5.6. AR, awake rest; AS, awake stimulation; CR, α -chloralose rest; CS, α -chloralose stimulation; HR, halothane rest; HS, halothane stimulation; PR, pentobarbital; UR1, urethane rest; UR2, urethane rest; US1, urethane stimulation; US2, urethane stimulation.

*Details in *SI Text*, section 1 and see Fig. 1A for comparison between calcCMR_{glc(ox)} and measCMR_{glc(ox)}.

[†] $\Sigma\delta_j$ was 1.90 mm (with $P_s = 4.81 \times 10^9 \text{ ATP/spike per neuron}$; see red circles in Fig. 1A).

[‡] $\Sigma\delta_j$ was 0.45 mm [with $P_s' = (0.45/1.90) \times P_s$; see orange circles in Fig. 1A].

square fitting to determine P_s and P_{ns} . An average P_s value of $4.81 \times 10^9 \text{ ATP/spike per neuron}$ was calculated by fitting Eq. 5 for all activity states in the rat, which is shown in Table 1. Because the neuronal activity data for some states in Table S1 were not available for all layers, P_s was estimated for those specific layers only [i.e., $(0.45/1.90) \times 4.81 \times 10^9 \text{ ATP/spike per neuron}$] (Table 2). Although the current P_s value is derived for the entire cortex, layer-specific P_s values are unlikely to vary by more than 50% of the average value. Fig. 1A shows the goodness of fit for Eq. 5 to the rat data (red circles) for an OGI of 5.6 with an R^2 value of 0.96 (gray line with $\sigma^2 = 0.0182$ for 11 states), indicating that the assumption of a constant value of P_s over the full activity range is well-supported.

P_{ns} in the Rat Somatosensory Cortex. The measured CMR_{glc(ox)} for the pentobarbital state in the rat (Table S1) was fitted to the E_{ns} term (Table 2). The constant E_{ns} term for all activity states was $0.76 \times 10^{17} \text{ ATP/s per centimeter}^3$, leading to average $P_{ns,N}$ and $P_{ns,A}$ values of $9.20 \times 10^8 \text{ ATP/neuron per second}$ and $6.85 \times 10^8 \text{ ATP/astrocytes per second}$, respectively, for an OGI range of 5.1–6.0 (20). These values of P_{ns} corresponded to an average R_{in} value of $74 \text{ M}\Omega$ (*SI Text*, section 2), which is well within the in vivo range measured for neurons and astrocytes (13, 14). As shown in Table 1, despite identical cortical densities of neurons and astrocytes, $P_{ns,N}$ and $P_{ns,A}$ were dissimilar, because slightly different Nernst potentials for Na^+ and K^+ and resting membrane potentials were used for neurons and astrocytes (*SI Text*, section 2), which has been done before (7, 8). However, similarity of contributions of astrocytes and neurons to nonsignaling energy consumption is in good agreement with measurements by ^{13}C MRS made under isoelectric pentobarbital anesthesia, supporting the accuracy of the derived values (2, 21).

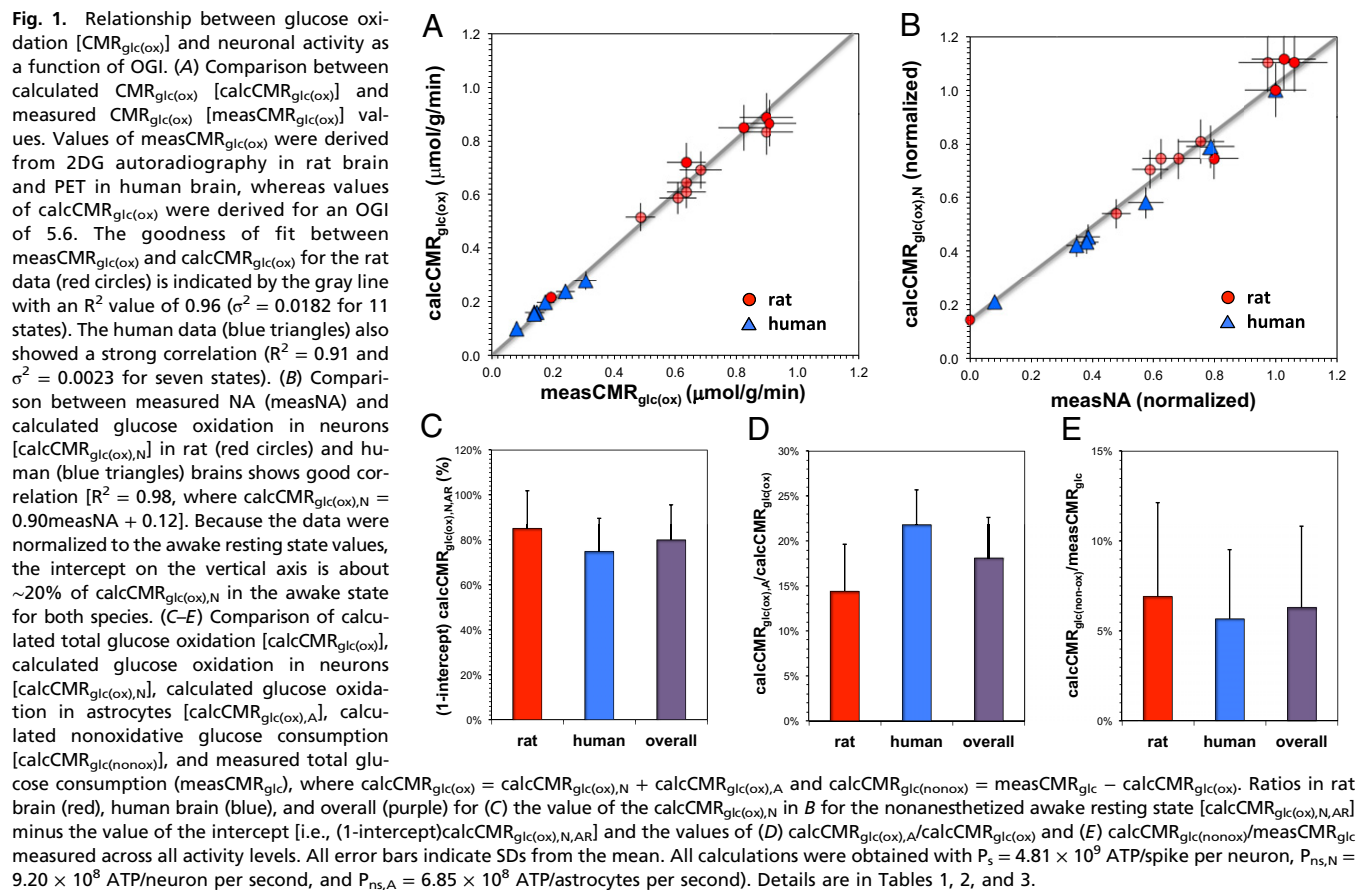
E_s and E_{ns} in the Human Visual Cortex. At present, there are insufficient studies in which electrical signaling in the human cerebral cortex (e.g., by single-unit recording) has been measured over a range of activity states to empirically derive P_s and P_{ns} , which was done for the rat cerebral cortex. To assess how different these values might be in the human, we used Eq. 1 with values for neuronal and glial densities determined for human and P_s and P_{ns} derived from the rat data, which required normalizing the awake BIS scale in humans to rat neuronal activity scale in the awake state (Eq. 6). Laminar firing rates in the human are not available, but according to the difference of $\langle f \rangle$ between rats and humans (Tables 2 and 3), we expect the cortical neuronal firing rate in humans to be lower than in rats. Although instantaneous neuronal firing rates in the awake human cerebral cortex can be quite variable from moment to moment (22), average rates estimated from steady-state measurements (23) are about 30–40% of the highest firing rates typically observed in the awake rat (Table S1). Firing rate measurements in the awake primate cortex are slightly higher than values found in human brain (24). Given that CMR_{glc} in awake primate cortex is about $0.5 \text{ }\mu\text{mol/g per minute}$ (25), which is between awake CMR_{glc} in rat and human (i.e., 0.8 vs. $0.3 \text{ }\mu\text{mol/g per minute}$, respectively), we expect that similar budget calculations can be made for primate cortex with the same P_s and P_{ns} values based on cellular density variations across the species (17). Although neuronal recordings in primate brain do not usually report quantitative firing rates (26), basic features of action potentials in the human cerebral cortex are quite similar to those features typically found in other animals, including rats and primates (27–29). Fig. 1A shows the goodness of fit for Eq. 5 to the human data (blue triangles) for an OGI of 5.6 with an R^2 value of 0.91 (gray line with $\sigma^2 = 0.0023$ for seven states), indicating that the assumption of a constant value of P_s derived from the rat is well-supported over the full activity range in the human.

Table 3. Calculated CMR_{glc(ox)} derived from neuronal activity in human visual cortex for OGI of 5.6

Behavioral state*	VGP	VGA	PRO	SEV	HAL	SLP	AWK
$\Sigma(\delta_i f_i \eta_{N,i}) (\times 10^3 \text{ spike.neuron.cm}^3 \text{ per centimeter}^3)$	282	1,192	1,317	1,306	1,959	2,674	3,407
$\Sigma(\delta_i f_i \eta_{N,i})/\Sigma\delta_j (\times 10^7 \text{ spike.neuron.s per centimeter}^3)$	0.12	0.51	0.56	0.56	0.83	1.14	1.45
$E_{ns} = \Sigma P_{ns,x} \times \eta_{N,x} (\times 10^{17} \text{ ATP/s per centimeter}^3)$	0.29	0.29	0.29	0.29	0.29	0.29	0.29
$E_s = P_s \times \Sigma(\delta_i f_i \eta_{N,i})/\Sigma\delta_j (\times 10^{17} \text{ ATP/s per centimeter}^3)$	0.06	0.24	0.27	0.27	0.40	0.55	0.70
$E_{tot} = E_{ns} + E_s (\times 10^{17} \text{ ATP/s per centimeter}^3)$	0.35	0.54	0.56	0.56	0.69	0.84	0.99
calcCMR _{glc(ox)} ($\mu\text{mol/g per minute}$)	0.10	0.15	0.16	0.16	0.20	0.24	0.28
measCMR _{glc(ox)} ($\mu\text{mol/g per minute}$)	0.08	0.14	0.15	0.14	0.18	0.24	0.31

Details in *Calculations*. To convert the EEG data in Table S2 into units of $\Sigma(\delta_i f_i \eta_{N,i})/\Sigma\delta_j$, simple conversions were needed with Eq. 6. The calculated CMR_{glc(ox)} [calcCMR_{glc(ox)}] was determined from Eq. 3. The measured CMR_{glc(ox)} [measCMR_{glc(ox)}] was determined from Eq. 4 assuming OGI of 5.6. AWK, awake; HAL, halothane; PRO, propofol; SEV, sevoflurane; SLP, non-REM sleep; VGA, acute vegetative; VGP, persistent vegetative.

*Details in *SI Text*, section 1 and see Fig. 1A for comparison between calcCMR_{glc(ox)} and measCMR_{glc(ox)}.



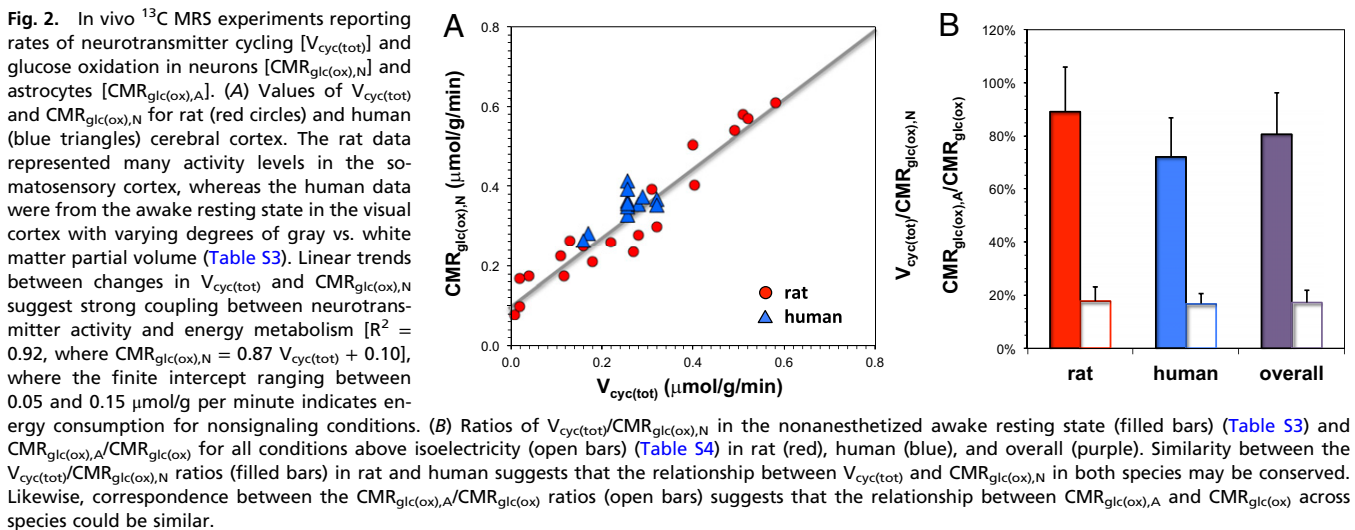
Relative Contributions of E_s and E_{ns} in the Resting Awake State. To represent the magnitude of E_{ns} vs. E_s in the resting awake state, we plotted the $\text{calcCMR}_{\text{glc}(\text{ox}),N}$ vs. the measured neuronal activity in a normalized scale (Fig. 1B). Because the intercepts on the $\text{calcCMR}_{\text{glc}(\text{ox}),N}$ vertical axis—which indicates the isoelectric condition—were ~0.1 and ~0.05 $\mu\text{mol/g}$ per minute for the rat and human, respectively (Fig. S3), or 15–20% of the $\text{calcCMR}_{\text{glc}(\text{ox}),N}$ in the awake state (Fig. 1B), the results suggest that a significant fraction of neuronal glucose oxidation in the awake state is dedicated for maintaining resting membrane potentials (Fig. 1C). Similarly, glial glucose oxidation is about ~20% of total glucose oxidation in the awake state (Fig. 1D). Based on reported OGI values (20), nonoxidative glucose consumption is about ~6% of total glucose consumption (Fig. 1E).

Comparison with ^{13}C MRS Studies. A similar linear relationship between neuronal activity and energy metabolism has been shown by results from ^{13}C MRS—a method that simultaneously measures rates of total neurotransmitter cycling [$V_{\text{cyc}(\text{tot})}$] and neuronal [$\text{CMR}_{\text{glc}(\text{ox}),N}$] as well as astrocytic [$\text{CMR}_{\text{glc}(\text{ox}),A}$] oxidative demand (2, 3). Fig. 2A shows the most up-to-date results from in vivo ^{13}C MRS studies in rats and humans (Tables S3 and S4), which illustrate nearly a 1:1 relationship between $\Delta V_{\text{cyc}(\text{tot})}$ and $\Delta \text{CMR}_{\text{glc}(\text{ox}),N}$ just beyond the isoelectric point when $V_{\text{cyc}(\text{tot})}$ approaches zero [i.e., gray line indicates an R^2 value of 0.92, $\text{CMR}_{\text{glc}(\text{ox}),N} = 0.87 V_{\text{cyc}(\text{tot})} + 0.10$]. Moreover, the in vivo ^{13}C MRS results of $V_{\text{cyc}(\text{tot})}/\text{CMR}_{\text{glc}(\text{ox}),N}$ and $\text{CMR}_{\text{glc}(\text{ox}),A}/\text{CMR}_{\text{glc}(\text{ox})}$ ratios in the awake state for both species, shown in Fig. 2B, show that neurons and astrocytes in the awake state demand about ~20% of oxidative ATP for nonsignaling factors. These results are similar to our budget calculations in Fig. 1.

Discussion

Comparison of Derived P_{ns} and P_s with Prior Calculations. There are large differences between $P_{ns,N}$ and $P_{ns,A}$ estimates for the rat by Attwell and Laughlin (7) and our empirically derived values (Table 1). Values of $P_{ns,N}$ and $P_{ns,A}$ are susceptible to starting assumptions (SI Text, section 2 and Fig. S1). This difference principally occurs, because Attwell and Laughlin (7) assumed $R_{in,N}$ and $R_{in,A}$ to be around 200 and 500 Ω , respectively, based on in vitro recordings (30, 31). However, our estimates of $R_{in,N}$ and $R_{in,A}$ values of 74 Ω are in close agreement with in vivo measurements (13, 14). Because P_{ns} depends on the reciprocal of R_{in} (SI Text, section 2), the higher $R_{in,N}$ and $R_{in,A}$ values by Attwell and Laughlin (7) are the main basis for their lower $P_{ns,N}$ and $P_{ns,A}$ estimates. Additionally, however, in the case of $P_{ns,N}$, there could also be differences in average neuronal density, which in the study by Attwell and Laughlin (7), were based on the mouse cortex (32), whereas our values were obtained from the rat cortex (15). The $P_{ns,N}$ and $P_{ns,A}$ values estimated by Lennie (8) for the human are approximately similar to our values, despite large differences in cell densities across species (Table 1). There are similar differences between P_s values for the rat by Attwell and Laughlin (7) and the human by Lennie (8) as discussed in detail below. However, in a recent ^{31}P MRS study of the human brain, Zhu et al. (33) estimated a P_s value of 4.7×10^9 ATP/neuron per second from measured cerebral metabolic rates of high-energy phosphate reactions catalyzed by ATPase. Assuming that, within 1 s, there is one spike in the awake brain, this value agrees well with P_s estimated in the current budget (Table 1).

Glial Energy Demand and Excitatory Vs. Inhibitory Neuronal Energy Requirements. The calculated astrocytic energy demand (Fig. 1D) is consistent with ^{13}C MRS results (Fig. 2B) but significantly higher than estimates from prior budgets (7, 8). The higher $E_{ns,A}$ values are because of using more recent values of astrocyte input



resistances (14). The in vivo results were fit well with the assumption of the major energetic changes with activity being in the neurons. Relatively constant astrocytic energetics (compared with neurons) as a function of overall cortical activity may reflect the energetics associated with maintaining the high astrocyte K^+ conductance dominating over additional functional demands (e.g., transporting glutamate and/or dealing with Ca^{2+} waves) as suggested by recent studies (34–37). ^{13}C MRS results, in support of these observations, show that energy demand of astrocytes changes considerably less than neuronal energy demand over wide activity levels (Table S4). However, the glial data are relatively limited compared with neuronal data, and future studies are needed to better understand glial functional energy requirements.

As in previous bottom-up calculations (7, 8), to derive P_s and P_{ns} , we could not separately include energy demand of inhibitory neurons, because the electrophysiological studies only included measurements of pyramidal neurons. Because $\text{CMR}_{\text{glc}(\text{ox}),\text{N}}$ contains the oxidative energy requirements of both excitatory and inhibitory neurons (15), the value of P_s likely reflects glutamatergic neurons working in conjunction with an ensemble of GABAergic neurons. Electrophysiological and ^{13}C MRS studies have found that, over the range of activity that we examined, both function and energy demand of GABAergic neurons is proportional to activity/demand of glutamatergic neurons (38, 39), consistent with the fractional contribution of excitatory and inhibitory neurons to P_s being constant throughout the activity range and similar to glutamatergic and GABAergic neuronal fractions measured morphologically (15).

Constancy of P_s and P_{ns} Across Activity Levels and Species. Previously, Karbowski (40) suggested that basal metabolic cortical differences across species could be described on allometric rationale. However, Herculano-Houzel (17) pointed out that absolute metabolic difference across species could be explained by neuronal number variations. Both Karbowski (40) and Herculano-Houzel (17) dealt with only the awake state values and the total metabolic rate (i.e., only E_{tot} in Eq. 1). In the current study, we partitioned E_{tot} for each activity level examined in terms of signaling (E_s) and nonsignaling (E_{ns}) components to test if P_s and P_{ns} are constant across species. Thus, neither E_s nor E_{ns} was assumed for any given state. E_s was derived based on the neuronal firing for a given state in each cortical layer for the rat and across the cortex in the human, whereas E_{ns} was based on leakiness of the cell membrane. To derive P_s , we fitted E_{tot} to measured $\text{CMR}_{\text{glc}(\text{ox})}$ data for each state, whereas to derive P_{ns} , we fitted E_{ns} to measured $\text{CMR}_{\text{glc}(\text{ox})}$ data for pentobarbital. Because barbiturates may also inhibit mitochondrial respiration (41) and if so, could lead to an overestimate of P_{ns} , we fitted the

data in Fig. 1B with and without the isoelectric pentobarbital data and found negligible differences in the slope, intercept, and goodness of fit [rat data: $\text{CMR}_{\text{glc}(\text{ox})} = 0.92$ neuronal activity (NA) + 0.13, $R^2 = 0.97$ with pentobarbital and $\text{CMR}_{\text{glc}(\text{ox})} = 0.94$ NA + 0.11, $R^2 = 0.93$ without pentobarbital]. A fixed P_{ns} does not necessitate a constant P_s . As shown in Fig. 1A and B, a constant value of P_s gave an excellent fit to the data. A nonconstant P_s , most likely a decrease at higher firing rates, would have shown itself as a deviation from the best linear fit. It should be recalled that bottom-up energy budgets predict that P_s and P_{ns} differ significantly across species (Table 1), and moreover, constancy of P_s and P_{ns} beyond the awake state had not been tested (7, 8).

The finding of a constant P_s across activity levels suggests that energy-consuming subcellular processes of the neuropil (e.g., ion fluxes associated with action potentials, pre- and postsynaptic potentials, vesicular exocytosis/endocytosis, neurotransmitter release/uptake, etc.) are all tightly coupled, ensuring that the fidelity of impulse trafficking across a synapse is maintained independent of signaling frequency. Although the mechanisms upholding this neurometabolic linearity are not understood, the rapid rate with which surrounding astrocytic end feet clear synaptic glutamate is probably a critical component (3). The similarity of energetic efficiency with regard to electrical (Fig. 1) and chemical (Fig. 2) events across different activity levels suggests that there are physiological factors that limit the energy associated with cortical signaling (42) and that, within the normal physiological range of neuronal signaling, the electrical and chemical events are complimentary (3). Assuming a constant energetic cost of Na^+ and K^+ pumping, there is a direct relationship between synaptic strength (i.e., average current induced by a signaling event at a synapse, which can be increased through either induced conductivity or higher probability of presynaptic glutamate release) and energy consumption at the synapse.

The stability of P_s and P_{ns} across species suggests that, early in evolution, the mammalian brain reached an optimum tradeoff between energy consumption and computational power at a cellular level (43). This constancy differs from most other tissues, where there is a decrease in cellular metabolic rate by a power of relative animal size (1). These findings imply that relative energy costs of fundamental features of cortical communication (e.g., action potentials, pre- and postsynaptic potentials, glial neurotransmitter and K^+ clearance, etc.) as well as physiological mechanisms for supplying mitochondrial energy for neuropil operations (e.g., hemoglobin, voltage-gated ion channels, glutamate and GABA receptors, and glucose and oxygen transport) are well-preserved through evolution (17, 28, 29, 44–49). A constant interspecies ATP demand of cortical activity emphasizes the relevance of animal testing in experimental neuroscience studies.

However, the approximately twofold difference in total cortical energy consumption between rats and humans may reflect limitations in blood flow in the human to supply oxygen and glucose and remove waste products and heat in relation to the number of cells that comprise each brain (50, 51).

Implications for fMRI and Resting Awake State Neuronal Activity. fMRI has become a major tool for mapping neuronal activity in humans and animals. An important question in fMRI studies is whether the change in signal during tasks, which is produced by changes in blood flow, blood volume, and oxygen consumption, directly reflects changes in neuronal activity (52). Our finding that a constant P_s fits experimental data both within and across species supports that measurements of the oxygen consumption component of fMRI can provide a quantitative measure of changes in neuronal activity. This conclusion is consistent with experimental studies using calibrated fMRI and multiunit recordings that have found a linear relationship between the average pyramidal cell signaling and regional oxygen consumption (4, 5, 36, 37). Our findings also show that the high level of neuronal activity in the resting awake state by ^{13}C MRS is consistent with metabolic

measurements of 2DG and PET as well as electrical activity measurements (spanning from EEG to extracellular recordings) for the rat and human, supporting proposals that resting state activity be incorporated into fMRI models of brain function (53). Because these results are relating macroscopic energy measurements to microscopic electrical events, we expect that the empirically derived values of P_s and P_{ns} can better guide bottom-up budgets of subcellular processes representing mammalian cortical function.

Materials and Methods

Tables S1 and S2 list values of neuronal activity and glucose consumption in rat and human for 11 and 7 different states, respectively, over a range of excitability (SI Text, section 1). In summary, the measured neuronal activity data were used to calculate $\text{CMR}_{\text{glc}(\text{ox})}$ and then compared with measured $\text{CMR}_{\text{glc}(\text{ox})}$ to determine values of P_s and P_{ns} (Tables 1, 2, and 3). The budget is described in Calculations (SI Text, section 2).

ACKNOWLEDGMENTS. We thank colleagues at Yale University and University of Sydney for insightful comments. This work was supported by National Institutes of Health Grants R01 MH-067528 (to F.H.), P30 NS-052519 (to F.H.), and R01 AG-034953 (to D.L.R.).

1. Aiello LC, Wheeler P (1995) The expensive-tissue hypothesis—the brain and the digestive-system in human and primate evolution. *Curr Anthropol* 36(2):199–221.
2. Sibson NR, et al. (1998) Stoichiometric coupling of brain glucose metabolism and glutamatergic neuronal activity. *Proc Natl Acad Sci USA* 95(1):316–321.
3. Hyder F, et al. (2006) Neuronal-glia glucose oxidation and glutamatergic-GABAergic function. *J Cereb Blood Flow Metab* 26(7):865–877.
4. Smith AJ, et al. (2002) Cerebral energetics and spiking frequency: The neurophysiological basis of fMRI. *Proc Natl Acad Sci USA* 99(16):10765–10770.
5. Maandag NJ, et al. (2007) Energetics of neuronal signaling and fMRI activity. *Proc Natl Acad Sci USA* 104(51):20546–20551.
6. Shulman RG, Rothman DL, Behar KL, Hyder F (2004) Energetic basis of brain activity: Implications for neuroimaging. *Trends Neurosci* 27(8):489–495.
7. Attwell D, Laughlin SB (2001) An energy budget for signaling in the grey matter of the brain. *J Cereb Blood Flow Metab* 21(10):1133–1145.
8. Lennie P (2003) The cost of cortical computation. *Curr Biol* 13(6):493–497.
9. Armstrong-James M, Fox K (1987) Spatiotemporal convergence and divergence in the rat S1 “barrel” cortex. *J Comp Neurol* 263(2):265–281.
10. Kossut M, Hand PJ, Greenberg J, Hand CL (1988) Single vibrissal cortical column in SI cortex of rat and its alterations in neonatal and adult vibrissa-deafferented animals: A quantitative 2DG study. *J Neurophysiol* 60(2):829–852.
11. Yang X, Hyder F, Shulman RG (1997) Functional MRI BOLD signal coincides with electrical activity in the rat whisker barrels. *Magn Reson Med* 38(6):874–877.
12. Buzsaki G (2006) *Rhythms of the Brain* (Oxford Univ Press, New York).
13. Dégenétais E, Thierry AM, Glowinski J, Gioanni Y (2002) Electrophysiological properties of pyramidal neurons in the rat prefrontal cortex: An in vivo intracellular recording study. *Cereb Cortex* 12(1):1–16.
14. Mishima T, Hirase H (2010) In vivo intracellular recording suggests that gray matter astrocytes in mature cerebral cortex and hippocampus are electrophysiologically homogeneous. *J Neurosci* 30(8):3093–3100.
15. Beaulieu C (1993) Numerical data on neocortical neurons in adult rat, with special reference to the GABA population. *Brain Res* 609(1–2):284–292.
16. Herculano-Houzel S, Mota B, Lent R (2006) Cellular scaling rules for rodent brains. *Proc Natl Acad Sci USA* 103(32):12138–12143.
17. Herculano-Houzel S (2011) Scaling of brain metabolism with a fixed energy budget per neuron: Implications for neuronal activity, plasticity and evolution. *PLoS One* 6(3):e17514.
18. Kent CD, Domino KB (2009) Depth of anesthesia. *Curr Opin Anaesthesiol* 22(6):782–787.
19. la Fougère C, et al. (2011) Where in-vivo imaging meets cytoarchitectonics: The relationship between cortical thickness and neuronal density measured with high-resolution $[^{18}\text{F}]$ flumazenil-PET. *Neuroimage* 56(3):951–960.
20. Shulman RG, Hyder F, Rothman DL (2001) Lactate efflux and the neuroenergetic basis of brain function. *NMR Biomed* 14(7–8):389–396.
21. Choi IY, Lei H, Grueter R (2002) Effect of deep pentobarbital anesthesia on neurotransmitter metabolism in vivo: On the correlation of total glucose consumption with glutamatergic action. *J Cereb Blood Flow Metab* 22(11):1343–1351.
22. Bitterman Y, Mukamel R, Malach R, Fried I, Nelken I (2008) Ultra-fine frequency tuning revealed in single neurons of human auditory cortex. *Nature* 451(7175):197–201.
23. Mukamel R, et al. (2005) Coupling between neuronal firing, field potentials, and fMRI in human auditory cortex. *Science* 309(5736):951–954.
24. Matsumoto K, Tanaka K (2004) The role of the medial prefrontal cortex in achieving goals. *Curr Opin Neurobiol* 14(2):178–185.
25. Shapiro HM, Greenberg JH, Reivich M, Ashmead G, Sokoloff L (1978) Local cerebral glucose uptake in awake and halothane-anesthetized primates. *Anesthesiology* 48(2):97–103.
26. Snodderly DM, Gur M (1995) Organization of striate cortex of alert, trained monkeys (*Macaca fascicularis*): Ongoing activity, stimulus selectivity, and widths of receptive field activating regions. *J Neurophysiol* 74(5):2100–2125.
27. Goldstein SR, Bak MJ, Oakley JC, Schmidt EM, Van Buren JM (1975) An instrument for stable single cell recording from pulsating human cerebral cortex. *Electroencephalogr Clin Neurophysiol* 39(6):667–670.
28. Williamson A, Spencer DD, Shepherd GM (1993) Comparison between the membrane and synaptic properties of human and rodent dentate granule cells. *Brain Res* 622(1–2):194–202.
29. Yu Y, Hill AP, McCormick DA (2012) Warm body temperature facilitates energy efficient cortical action potentials. *PLoS Comput Biol* 8(4):e1002456.
30. Clark BA, Mobbs P (1994) Voltage-gated currents in rabbit retinal astrocytes. *Eur J Neurosci* 6(9):1406–1414.
31. Hutcheon B, Miura RM, Puil E (1996) Models of subthreshold membrane resonance in neocortical neurons. *J Neurophysiol* 76(2):698–714.
32. Braitenberg V, Schüz A (1998) *Cortex: Statistics and Geometry of Neuronal Connectivity* (Springer, Berlin), 2nd Edn.
33. Zhu XH, et al. (2012) Quantitative imaging of energy expenditure in human brain. *Neuroimage* 60(4):2107–2117.
34. Hirase H, Qian L, Barthó P, Buzsáki G (2004) Calcium dynamics of cortical astrocytic networks in vivo. *PLoS Biol* 2(4):E96.
35. Dombeck DA, Khabbaz AN, Collman F, Adelman TL, Tank DW (2007) Imaging large-scale neural activity with cellular resolution in awake, mobile mice. *Neuron* 56(1):43–57.
36. Sanganahalli BG, Herman P, Blumenfeld H, Hyder F (2009) Oxidative neuroenergetics in event-related paradigms. *J Neurosci* 29(6):1707–1718.
37. Herman P, Sanganahalli BG, Blumenfeld H, Hyder F (2009) Cerebral oxygen demand for short-lived and steady-state events. *J Neurochem* 109(Suppl 1):73–79.
38. Shu Y, Hasenstaub A, Duque A, Yu Y, McCormick DA (2006) Modulation of intracortical synaptic potentials by presynaptic somatic membrane potential. *Nature* 441(7094):761–765.
39. Patel AB, et al. (2005) The contribution of GABA to glutamate/glutamine cycling and energy metabolism in the rat cortex in vivo. *Proc Natl Acad Sci USA* 102(15):5588–5593.
40. Karbowiak J (2007) Global and regional brain metabolic scaling and its functional consequences. *BMC Biol* 5:18.
41. Anderson CM, et al. (2002) Barbiturates induce mitochondrial depolarization and potentiate excitotoxic neuronal death. *J Neurosci* 22(21):9203–9209.
42. Niven JE, Laughlin SB (2008) Energy limitation as a selective pressure on the evolution of sensory systems. *J Exp Biol* 211(Pt 1):1792–1804.
43. Laughlin SB, Sejnowski TJ (2003) Communication in neuronal networks. *Science* 301 (5641):1870–1874.
44. Storz JF (2007) Hemoglobin function and physiological adaptation to hypoxia in high-altitude mammals. *J Mammal* 88(1):24–31.
45. Vacher H, Mohapatra DP, Trimmer JS (2008) Localization and targeting of voltage-dependent ion channels in mammalian central neurons. *Physiol Rev* 88(4):1407–1447.
46. Dingledine R, Borges K, Bowie D, Traynelis SF (1999) The glutamate receptor ion channels. *Pharmacol Rev* 51(1):7–61.
47. Young AB, Chu D (1990) Distribution of Gaba-A and Gaba-B receptors in mammalian brain—potential targets for drug development. *Drug Dev Res* 21(3):161–167.
48. Pessin JE, Bell GI (1992) Mammalian facilitative glucose transporter family: Structure and molecular regulation. *Annu Rev Physiol* 54:911–930.
49. Hyder F, Shulman RG, Rothman DL (1998) A model for the regulation of cerebral oxygen delivery. *J Appl Physiol* 85(2):554–564.
50. Trübel HK, Sacolick LI, Hyder F (2006) Regional temperature changes in the brain during somatosensory stimulation. *J Cereb Blood Flow Metab* 26(1):68–78.
51. Rango M, Arighi A, Bresolin N (2012) Brain temperature: What do we know? *NeuroReport* 23(8):483–487.
52. Hyder F (2004) Neuroimaging with calibrated fMRI. *Stroke* 35(11 Suppl 1):2635–2641.
53. Shulman RG, Hyder F, Rothman DL (2009) Baseline brain energy supports the state of consciousness. *Proc Natl Acad Sci USA* 106(27):11096–11101.